CHEMISTRY OF MATERIALS

pubs.acs.org/cm

Article

Thermal Atomic Layer Etching Process for 2D van der Waals Material $CrPS_4$

Marissa D. Pina Matthew P. Whalen John Q. Xiao and Andrew V. Teplyakov

Cite This: https://doi.org/10.1021/acs.chemmater.4c01606

Read Online

ACCESS | Metrics & More | Article Recommendations | Supporting Information

ABSTRACT: Preparing two-dimensional (2D) van der Waals materials with atomic-level precision remains a major hurdle, preventing both a number of fundamental explorations of quantum phenomena and a wider range of applications that can be based on a variety of their properties. It is especially challenging for tertiary materials, such as $CrPS_4$, which cannot be produced by controlled deposition but could be managed by etching or thinning in a layer-by-layer approach. Thin flakes of this material can display ferromagnetic or antiferromagnetic behavior depending on the number of layers since the crystal exhibits A-type antiferromagnetic ordering. In order to understand the magnetism down to the monolayer limit and the dynamic excitations in magnons and excitons, and to eventually make devices based on this and similar materials viable, well-controlled layered structures must be produced. The existing methods for controlling $CrPS_4$ thickness, such as mechanical and liquid exfoliation, are not well controlled and are prone to introducing damage to the crystal structure. In this study, we show that thermal atomic layer etching (ALE) can be used to controllably etch the 2D crystals of this material without noticeable contamination. As a starting point, $CrPS_4$ flakes were mechanically exfoliated onto a solid substrate and mounted in an ultra-high vacuum chamber. ALE process consisted of a chlorine gas dose from a solid-state halogen doser followed by exposure to gas-phase acetylacetone (acacH). This ALE approach showed an etch rate of approximately 0.10 nm/cycle at 450 K, confirmed by atomic force microscopy. The etch rate is noticeably faster for the flakes with a large number of defects. The overall process is highly temperature-dependent with a narrow window for successful application.

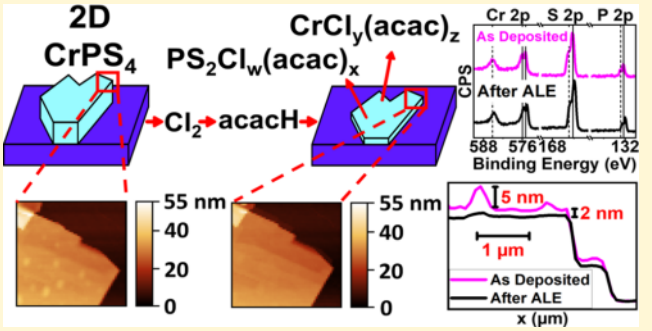

INTRODUCTION

Two-dimensional (2D) van der Waals ferromagnets display a rare combination of unusual properties that offer a platform to test fundamental physics, to explore and apply quantum phenomena, and also to advance a number of applications including imaging, gas and biosensing, photovoltaics, spintronics, and microelectronics.[1−5] However, many 2D van der Waals ferromagnets are particularly susceptible to degradation in ambient conditions through hydration or oxidation.[5] One 2D ferromagnet that has been shown to resist oxidation is chromium thiophosphate ($CrPS_4$).[5]

$CrPS_4$ is a ternary transition metal chalcogenide (TTMC). Monolayer and few-layer flakes of this material are of interest because they have unique properties in contrast to the bulk crystal. This includes A-type antiferromagnetism, which is predicted to be energetically most favorable for $CrPS_4$, meaning that adding a single layer of the material causes alternation between antiferromagnetic and ferromagnetic behavior.[6−8] $CrPS_4$ has a puckered structure. Each layer has a spacing of 0.61−0.62 nm, which varies based on the substrate.[6] The general structure of the $CrPS_4$ layers is presented in the inset of Figure 1.

Achieving precise control over the preparation of few-layer and monolayer flakes of 2D materials is a prerequisite for understanding fundamental quantum phenomena; however, the technology based on this control is also immediately relevant to applications in components of integrated circuits. As the critical dimensions of these components have decreased substantially every year following Moore's law, the semiconductor industry is rapidly evolving beyond Moore's law to include three-dimensional structures. The nodes in the current gate-all-around (GAA) technology have reached sub-3 nm dimensions, and it is expected that the critical dimensions will reach sub-1 nm by 2035, allowing 2D materials (such as $CrPS_4$ with its interplanar distance of 0.61 nm) to serve as the perfect templates for bottom-up manufacturing.[9] In addition to this advantage, 2D materials can potentially be prepared with low-

Received: June 8, 2024
Revised: July 23, 2024
Accepted: July 24, 2024

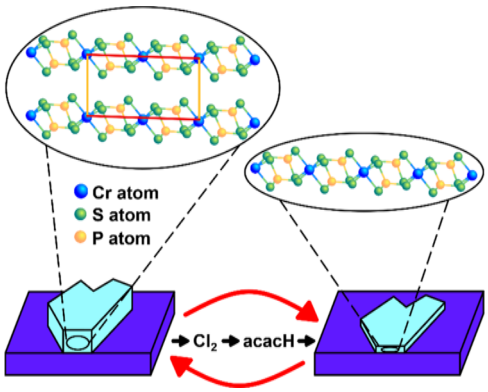

Figure 1 Schematic of the atomic layer etching (ALE) of $CrPS_4$ using half-cycles of Cl_2 and acacH. The zoomed-in areas show the structure of 2D $CrPS_4$. The interlayer spacing (represented by the yellow line) is 0.614 nm.[6] The red line depicts one of the lattice constants for the $CrPS_4$ unit cell and is 1.0871 nm.[6]

defect densities. In traditional materials scaled to the same dimensions, defects, such as dangling bonds and atomically rough surfaces, could lead to a decrease in charge carrier mobility and an increase in short channel effects.[9] Another great advantage of using these materials is the potential to create perfect interfaces between the components or elements of a device since they bind to other materials through van der Waals forces. Van der Waals heterostructures (vdWHs) do not suffer from lattice mismatching, and most of the time do not require extreme treatments or high temperatures for preparation.[9] With new paradigms continuously being developed in microelectronics, vdWHs are also highly viable options for exploring novel and unconventional device concepts.[9]

Therefore, it is important to controllably and conformally etch 2D materials, including $CrPS_4$ with atomic or at least layer-by-layer precision following its deposition. Mechanical exfoliation is commonly used to deposit thinned flakes onto a substrate, but the resulting flakes often have rough surfaces and vary tremendously in thickness and width, which can be affected by the choice of substrate.[10,11] $CrPS_4$ flakes can be mechanically exfoliated onto silicon and SiO_2 substrates, but gold substrates open doors for easily exfoliating large few-layer and even monolayer flakes.[12−18] Liquid exfoliation often results in a wide distribution of sizes and shapes and could damage the crystals; chemical vapor deposition (CVD) has not been heavily explored for this material, but CVD of other 2D materials like $MoSe_2$ often results in poor-quality monolayers; and chemical vapor transport (CVT) can only be used to create relatively large crystals that require subsequent thinning.[10,11,19,20]

Thermal atomic layer etching (ALE) could potentially provide a much more controlled and scalable method for thinning $CrPS_4$ flakes, along with a way to eliminate defects and produce a nearly atomically flat surface.[21] It is worth noting that ALE approaches have been proposed for a number of binary 2D materials; however, they mostly rely on plasma- or laser-assisted removal of material, which may cause physical damage to the surface and the layers.[22,23] Recently reported thermal ALE of MoS_2 was achieved at 250 °C by a combination of MoF_6 and H_2O.[24] In that set of investigations, the amorphous material was etched successfully but etching of the highly crystalline, low-defect areas of MoS_2 flakes was very slow, with a reported rate below 0.02 nm/cycle. Another method for etching MoS_2 with steam treatment has been reported to produce different edge morphologies of this material.[25] This observation brings up the question of anisotropic etching and the role of defects and edges in the ALE of 2D materials in general, suggesting that the same challenges may be present for the thermal ALE of crystalline $CrPS_4$.

Complicated 2D materials composed of more than two elements are even more challenging to grow or etch than binary materials since additional complexity could lead to unwanted enrichment or depletion of the material components, leading to substantial changes in physical properties. It has been demonstrated previously by our group that thermal ALE of tertiary material CoFeB can be optimized to maintain the concentrations of each element in the alloy without affecting its magnetic properties, but this has never been shown for tertiary 2D van der Waals materials.[26]

In designing the chemistry for thermal ALE, all of the above-mentioned issues have to be considered. In addition, the reactions proposed for individual elements of the alloy or ternary material must be viable. For example, the first half-cycle of the thermal ALE process is often oxidation or chlorination.[27,28] The second half-cycle most of the time involves an organic ligand that makes a volatile compound, which can easily desorb from the surface.[27,28] In previous work, our group demonstrated the effectiveness of Cl_2 and acacH as reactants in half-reactions for the thermal ALE of a CoFeB alloy. The volatile acetylacetonates of Co and Fe are very well-known, and they were expected to play a role in ALE. However, mixed-ligand compounds were formed for both light (B), and heavy (Co, Fe) elements in the form of $M(acac)_xCl_y$ as shown by temperature-programmed desorption (TPD) measurements.[29,30] In fact, the formation of volatile acetylacetonates of Co and Fe does occur, but at much higher temperatures compared to the ones used in ALE.[29,31−33]

In a similar approach, one could start considering $Cr(acac)_3$ and H_3PS_4 as potential products of the ALE of $CrPS_4$. $Cr(acac)_3$ is a stable compound that is capable of subliming at 500 K,[34] providing a possibility of etching in a non-self-limiting regime (also considered below). The key, however, is to find the chemistry that will be capable of removing all of the elements of the target 2D material with similar rates at similar conditions and to perform this using coreactants leading to true atomic-level control. Chlorine has been shown to weaken the bonds between the transition metal it is attached to the surrounding matrix.[35] Therefore, chlorination should allow for controlled removal of the entire layer of $CrPS_4$ by combining this step with a dose of acacH, even if the resulting species are, in fact, compounds with mixed ligands ($M(acac)_xCl_y$) rather than $Cr(acac)_3$. The specific chemistry could be the subject of a separate investigation; however, one can consider chemical reactions leading to the formation of various mixed-ligand compounds. Some of these potential reaction pathways may be based on the processes including the following reactions:

$$CrPS_4 \quad 5Cl_2 \quad 2acacH \rightarrow CrCl\ acac)_2 \quad PCl_3 \quad 2S_2Cl_2 \quad 2HCl \tag{1}$$

$$CrPS_4 \quad 3Cl_2 \quad 4acacH \rightarrow CrCl\ acac)_2 \quad HPS_2\ acac)_2 \quad S_2Cl_2 \quad 3HCl \tag{2}$$

https://doi.org/10.1021/acs.chemmater.4c01606
Chem Mater XXXX XXX XXX−XXX

$$CrPS_4 \quad Cl_2 \quad 3acacH \rightarrow CrCl\ acac)_2 \quad HPS_2Cl\ acac) \quad S_2Cl_2 \quad 2HCl \quad (3)$$

In this study, we will show that we can controllably etch $CrPS_4$ and that defects play a major role in the process, as highly defective features are etched at substantially higher rates than those of terraces. A combination of chlorine (from a solid-state doser) and gas-phase acetylacetone (acacH) dosed sequentially, as shown schematically in Figure 1, yields an ALE rate of approximately 0.10 nm/cycle. We have identified the species formed on the surface of $CrPS_4$ by these etchants spectroscopically, but only a combination of both results in atomic-level control. This process is highly temperature-dependent, since ALE cycles performed at 420 K do not result in any etching while increasing the temperature to 450 K does. Further increase in the temperature and acacH pressure apparently leads to a substantially faster etching rate, but proceeds beyond thermal ALE regime.

EXPERIMENTAL SECTION

Sample Preparation: Mechanical Exfoliation. Exfoliations conducted without gold employed <100> p-type (boron), single-side polished, prime-grade CZ Virgin Silicon Wafers purchased from Ted Pella or 500 μm thick <100> p-type, single-side polished silicon wafers with 300 nm SiO_2 deposited on top. Preceding exfoliation, the wafer was cleaved into square chips measuring approximately 1 cm × 1 cm. The exfoliation procedure was carried out on the polished side of the silicon chips after blowing the chip with N_2 for 10−15 s to remove large contaminants. This procedure begins by placing large bulk crystals of $CrPS_4$ (HQ Graphene) onto blue tape (ProTapes Nitto SPV224 PVC Vinyl tape). The tape was folded onto itself 3−5 times to cleave the crystal into smaller pieces on the tape. These freshly exposed surfaces were gently pressed onto the surface of the substrate for about a minute. This was done quickly after cleaving the crystals to prevent contamination of the fresh surface, which we found limits the size of the exfoliated flakes. The tape was gently peeled from the surface of the substrate, leaving flakes of varying size on the surface of the silicon wafer.

Sample Preparation: Gold Assisted Exfoliation. Exfoliations conducted with gold to obtain flakes of larger sizes used 500 μm thick <100> p-type, single-side polished silicon wafers with 300 nm SiO_2 deposited on top. The wafer was cleaved into 1 cm × 1 cm squares polished side up. These chips were blown with N_2 before being loaded into the sputtering chamber. Gold deposition was performed at room temperature by using DC magnetron sputtering at 1×10^{-6} Torr base pressure. A 2 nm titanium adhesion layer was deposited at 40 W power followed by 7.5 nm of gold at 15 W power. Within approximately 5 min of removing the film from the vacuum, $CrPS_4$ was exfoliated following the procedure described above. The gold-assisted exfoliation procedure is conducive to producing flakes of $CrPS_4$ of larger lateral dimensions that are more amenable for selected investigations; however, it is also much more elaborate than the simple mechanical exfoliation. Since the main target of the current work is an investigation of the ALE regime in relatively thick (20−30 nm) flakes, it was assumed that the substrate does not significantly affect the ALE process. Further work will be needed to determine the role of the substrate when only a few monolayer flakes are the starting point for ALE.

Reactor 1. All ALE experiments were performed in a near ultrahigh vacuum chamber (UHV) with a base pressure below 2×10^{-8} Torr. The chamber has a bake-out period, where a temperature of 375 K is maintained for 3 days, followed by a degassing period before any experiments are performed. The UHV chamber is equipped with a differentially pumped quadrupole residual gas analyzer mass spectrometer (MS, Hiden Analytical). Samples were chlorinated *in situ* using a home-built solid-state electrochemical chlorine source based on silver chloride and cadmium chloride.[30,36,37] This source provides precise fluxes of Cl_2 gas molecules, and the corresponding surface coverage on a sample can be calibrated spectroscopically, as briefly described below. The organic compound was degassed by repeated dosing into the chamber, until the mass spectrum showed the expected m/z fragments. The pressure was monitored by a cold cathode vacuum gauge.

Atomic Layer Etching. The first ALE half-cycle consists of a 40 min chlorine dose [5 μA and 70−90 V applied] at 450 K. These dosing parameters were shown to saturate a substrate surface with approximately a monolayer of chlorine, as determined by previous *in situ* Auger electron spectroscopy measurements.[30] The second ALE half-cycle consists of a 1500 Langmuir (L) acacH dose (5×10^{-6} Torr for 5 min) at 450 K. Liquid acacH (2,4-pentanedione, 99 purity) from Thermo Scientific Chemicals was connected to a leak valve and used to dose acacH onto the sample in the gas phase. The mass spectrum was collected *in situ* to ensure that the acacH was degassed and produced the expected mass spectrum verified with the NIST library.[38] A nearly identical set of ALE experiments was performed at 420 K.

Reactor 2. A high vacuum (HV) chamber was used to dose acacH on the surface for *ex situ* analysis. The high vacuum chamber was equipped with a mechanical pump and a turbo pump. The base pressure was 10^{-6} Torr. The pressure was monitored with a cold cathode vacuum gauge.

Dosing acacH in High Vacuum. $CrPS_4$ flake samples were mounted in a high vacuum experimental setup. Liquid acacH (2,4-pentanedione, 99 purity) from Thermo Scientific Chemicals was dosed via a leak valve into the chamber at a pressure of 0.1 Torr. The doses were completed at room temperature, 415 K, and above 450 K.

Sample Characterization. All sample characterization was completed at the Surface Analysis Facility (SAF), Advanced Materials Characterization Lab (AMCL), or Keck Center for Advanced Microscopy and Microanalysis at the University of Delaware.

X-ray photoelectron spectroscopy (XPS) was performed by using a Thermo Scientific K- X-ray Photoelectron Spectrometer, and the results were used to determine the composition of the sample surface. The XPS uses a 180° double-focusing hemispherical analyzer, an Al−K X-ray monochromatic source ($h\nu$ = 1486.6 eV) at a 35.3° takeoff angle with respect to the analyzer, and an adjustable 30−400 μm spot size. Survey spectra were collected over the energy range of 0−1000 eV. High-resolution spectra were collected with 0.1 eV resolution and a pass energy of 20 eV. All spectra were calibrated by setting the C 1s peak to 284.6 eV. CasaXPS (version 2.3.25PR1.0) software was used for XPS spectra analysis.[39]

Atomic force microscopy (AFM) imaging was completed using an Anasys Nano IR2 in tapping mode. The AFM tips are Sb-doped Si with a 50 nm Au coating and a radius of 20 nm. The AFM tips (PR-EX-TNIR-A-10) have a resonance frequency of 75 ± 15 kHz and a spring constant of 1−7 N/m. The resulting height profiles were used to determine the flake thickness change after ALE. The images were analyzed using Gwyddion software (version 2.64).

Time-of-flight secondary ion mass spectrometry (ToF-SIMS) surface spectra were obtained using an IONTOF TOF.SIMS 5 system, which employs a 30 keV Bi cluster ion source. A low-energy electron flood gun is used for charge compensation during analysis. The surface spectra were used to determine what species were present on the surface of the sample. SurfaceLab 7 (version 7.3) software was used to analyze all of the ToF-SIMS data.

Cross-sectional transmission electron microscopy (TEM) samples were prepared using a focused ion beam-scanning electron microscopy (FIB-SEM) system. The cross-sectional TEM samples were prepared by using an AURIGA 60 Crossbeam FIB-SEM dual beam instrument. TEM was performed using a 20−200 kV thermionic Thermo Scientific Talos F200C TEM. The TEM images were used to characterize the Au substrate under a $CrPS_4$ flake after ALE experiments.

An optical microscope (Olympus BX60 Brightfield/Darkfield Transmitted and Reflected Light Microscope) was used to collect optical images of the flakes of interest.

https://doi.org/10.1021/acs.chemmater.4c01606
Chem Mater XXXX XXX XXX−XXX

RESULTS AND DISCUSSION

Characterization of the $CrPS_4$ Surface. Although it is assumed that $CrPS_4$ is very stable and resistant to oxidation, it is important to confirm that ambient conditions do not substantially affect the chemistry and composition of the surface of this material and that the etching components (Cl_2 and acacH) would adsorb directly onto the clean surface. XPS and ToF-SIMS were used to characterize the $CrPS_4$ flakes before and after the etching experiments. Figure 2 shows an optical image of a relatively thick flake of $CrPS_4$ along with a few flakes that are only several layers thick, as indicated by the arrows. The ToF-SIMS ion images for selected ions zoom in on a 500 μm area to compare the chemistry of the thick and thin flakes shown in the optical image. As expected, the Cr^+, P^-, and S^- species are clearly visible on the flakes but not on the substrate. It is also obvious that the ion images provide information about the surface of the $CrPS_4$ material as no substantial difference in intensity of the key representative ions is noticeable between thick and thin flakes. The Au^+ signal from the substrate is clearly blocked by the $CrPS_4$ material.

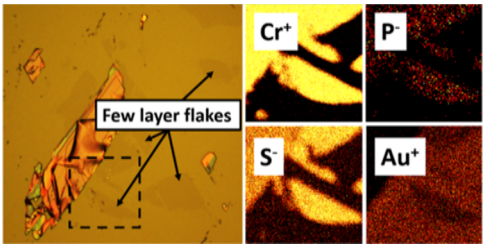

Figure 2 Optical image (left) of few-layer $CrPS_4$ flakes neighboring a thick flake as well as the corresponding 500 μm wide ToF-SIMS ion images (right). The black-dashed box on the optical image is the 500 μm wide raster area that was scanned to obtain the ToF-SIMS ion images. The flakes were deposited on a thin Au film. The same area was scanned for both negative and positive ion collection. All expected species (Cr^+, P^-, and S^-) are clearly visible on the flake areas and absent on the substrate. The Au^+ signal is completely obstructed by the thick flake, but less so by the few-layer flakes.

Quantitative information about the composition of the $CrPS_4$ flakes and the oxidation states of the corresponding elements is obtained by XPS. Figure 3 compares the XPS spectra of the $CrPS_4$ single crystal (no substrate) right after its cleavage to minimize exposure to ambient conditions and after extended exposure to ambient conditions. These spectra are also compared to the XPS of $CrPS_4$ flakes deposited on Au by mechanical exfoliation and XPS of the flakes deposited on Si after an ALE experiment. This comparison confirms the presence of Cr, P, and S and suggests that exposure to ambient conditions does not appear to affect the chemistry of this material. Specifically, the high-resolution Cr 2p, P 2p, and S 2p spectral regions do not exhibit any changes after extended exposure to ambient conditions, regardless of whether the material is in the form of a single crystal or a flake. The ratio of these elements does not change among these samples, confirming that both exfoliation and ALE maintain the overall stoichiometry of $CrPS_4$.

An additional comment can be made about the oxidation states of the elements within this material. The positions of the chromium features, including characteristic spin−orbit coupling and a unique additional splitting of the Cr $2p_{3/2}$ feature, confirm that Cr is in a +3 oxidation state.[6,40] The two peaks in the P 2p spectral region correspond to spin−orbit-coupled peaks in phosphosulfides[40] and prove that there is no noticeable oxidation of this element, as the potential peaks corresponding to phosphates are fully absent above ~133 eV.[41−46] The positions of the spin−orbit-coupled peaks in the S 2p spectral region are consistent with sulfur in $CrPS_4$[40] but are not consistent with elemental sulfur ($2p_{3/2}$ and $2p_{1/2}$ peaks expected at 164 and 165 eV, respectively) or sulfur oxides (expected above ~166 eV).[47−51] Thus, analysis of the XPS spectra presented in Figure 3 supports the observation that the flakes transferred onto the support material by exfoliation and the flakes after an ALE experiment are representative of $CrPS_4$ and are not affected by exposure to ambient or ALE conditions. Most notably, no surface oxidation is observed by XPS, making it possible to apply the same ALE chemistry to the starting surface and to the underlying layers to control the thicknesses of these supported flakes. One can notice that the sample with $CrPS_4$ flakes subjected to ALE shown in Figure 3d appears to exhibit a very small shift in binding energy compared to the samples in Figure 3a−c. This small shift is most likely caused by the substrate modified by ALE steps, as the flakes occupy a very small portion of the sample surface and the positions of all of the peaks are always calibrated by the dominant C 1s feature. This small shift does not affect the conclusions that all of the elements comprising the $CrPS_4$ flakes are not affected noticeably by exposure to ambient conditions and that their oxidation states remain the same after ALE.

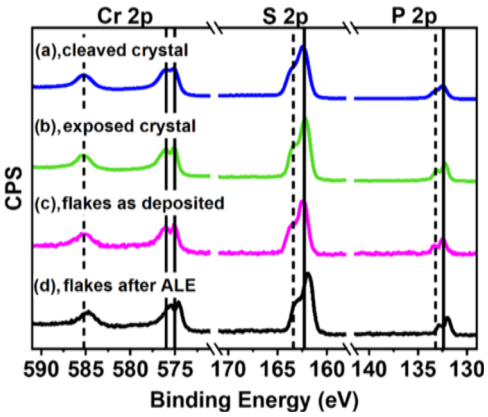

Figure 3 High-resolution XPS scans of the Cr 2p, S 2p, and P 2p binding energy regions for (a) freshly cleaved single crystal with minimal exposure to ambient conditions, (b) the crystal that was exposed to ambient conditions for several days, (c) the exfoliated $CrPS_4$ flakes as deposited on an Au film, and (d) the exfoliated flakes on a Si substrate after an ALE experiment. The black reference lines indicate the actual binding energies for each orbital (Cr 2p- 575.0, 576.0, 585.2 eV; S 2p- 162.3 and 163.4 eV; and P 2p- 132.4 and 133.2 eV). The solid reference lines indicate the positions of the $2p_{3/2}$ peaks, and the dashed reference lines indicate the positions of the $2p_{1/2}$ peaks.

Individual Half Cycles for ALE of $CrPS_4$. Given the confirmed chemical stability of the supported $CrPS_4$ flakes, before the roadmap to a successful thermal ALE can be offered, it is important to test whether the proposed chlorination and acacH exposure could actually modify the surface of this material within the same temperature window. The challenge with confirming chlorination is that it has to be demonstrated specifically on the flakes rather than on the support material. To confirm that the $CrPS_4$ flakes can be chlorinated, chlorine

https://doi.org/10.1021/acs.chemmater.4c01606
Chem Mater XXXX XXX XXX−XXX

was dosed on the flakes at 420 K in UHV. ToF-SIMS surface ion images (Figure 4) show that there is definitely an overlap between the images of Cr^+ and Cl^- after dosing Cl_2 although some amount of chlorine is indeed present on the Au surface of the support. Thus, the fact that flakes can be chlorinated is confirmed. No etching was observed for Cl_2 exposure in UHV within our range of conditions; however, further investigations will be needed to determine if Cl_2 gas can etch $CrPS_4$ at higher temperatures and pressures.

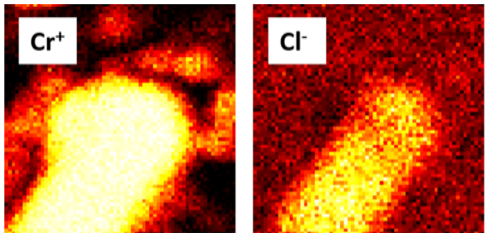

Figure 4 ToF-SIMS Cr^+ (m/z = 51.940) and Cl^- (m/z = 34.970) ion images of a $CrPS_4$ flake on an Au film after UHV chlorination at 420 K. The same flake was scanned for both negative and positive ion collection.

To confirm the reactivity of acacH with $CrPS_4$ flakes on SiO_2 and Au substrates, 0.1 Torr of acacH was dosed onto the samples for 50 min in a high vacuum chamber. The samples were heated to 295 K, 415 K, or above 450 K during the acacH doses. In this experimental setup, reading precise surface temperatures above 450 K was challenging, and the actual surface temperature in this experiment was between 450 and 500 K. ToF-SIMS surface spectra taken after each dose show that acacH does strongly interact with the $CrPS_4$ surface. Figure 5 clearly shows the presence of acac-based chromium-containing species. At 295 K, the formation of these species is noticeable; but at 415 K, they are very clearly present. Additionally, Figure 5 summarizes the correct identification of

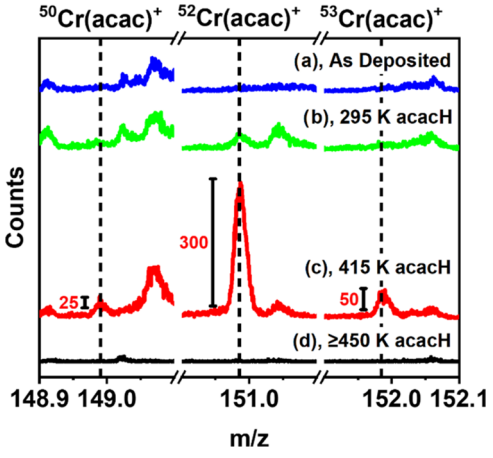

Figure 5 ToF-SIMS surface spectra of m/z ranges corresponding to an acac ligand bound to the most abundant chromium isotopes ($^{50}Cr(acac)^+$, $^{52}Cr(acac)^+$, and $^{53}Cr(acac)^+$). Spectra are provided for (a) the as-deposited $CrPS_4$ flakes, and (b) flakes after dosing acacH at room temperature, (c) 415 K, and (d) ≥450 K (controlling precise surface temperature above 450 K was challenging, and the actual surface temperature in this experiment was between 450 and 500 K). The black-dashed reference lines specify the exact m/z for each of the indicated species (148.991, 150.985, and 151.985).

$Cr(acac)^+$ based on the isotope abundances of ^{50}Cr (2.37), ^{52}Cr (83.8), and ^{53}Cr (9.50). Identifying $Cr(acac)_x^+$ based on Cr isotope ratios was especially important because any given peak can be attributed to an abundance of different possible species, especially at higher m/z. Similar results were collected for $Cr(acac)_2^+$ species (Figure S1). On the other hand, no confirmation of the presence of $Cr(acac)_3^+$ (Figure S2) could be obtained with these experiments at any temperatures studied. This observation suggests that $Cr(acac)_3$ does not form at temperatures below 450 K on the $CrPS_4$ surface, but above 450 K, it could potentially form and then desorb.[34] Interestingly, if the surface temperature is raised above the nominally measured 450 K, all of the spectral signatures of $Cr(acac)_x^+$ disappear, suggesting either desorption of acac-containing species or possibly acac decomposition.

That last observation appears to offer the possibility of continuous etching of $CrPS_4$ by acacH at elevated pressures and temperatures. Indeed, as summarized by AFM analysis of the sizes of the flakes before and after acacH exposure in Figure 6, exposure of $CrPS_4$ flakes to large doses of acacH

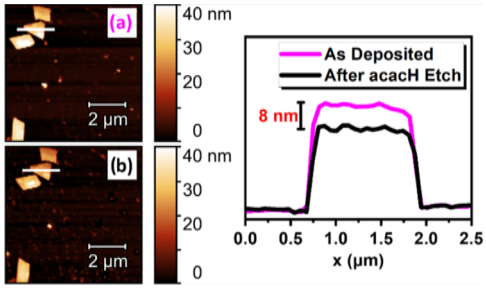

Figure 6 Etching of $CrPS_4$ flakes on an Au film by a 50 min 0.1 Torr acacH dose in HV at 450 K (controlling precise surface temperature above 450 K was challenging, and the actual surface temperature in this experiment is between 450 and 500 K). AFM height images are provided for the $CrPS_4$ flake sample before (a) and after (b) the etching experiment. The total thickness etched was 8 ± 2 nm after the experiment (based on an analysis of 29 points). The line profiles correspond to the white lines drawn over the triangular flakes in each image.

under high vacuum at a temperature between 450 and 500 K results in continuous etching. In this specific experiment, a single dose of 0.1 Torr of acacH for 50 min resulted in a decrease of the flake thickness by 8 nm, clearly a regime that is much faster than ALE and is not self-limiting. This regime change is a subject of further investigation; however, dosing 5 × 10^{-6} Torr acacH for 5 min at 450 K in a UHV setup (where the temperature is monitored with much higher precision) and repeating this dose 30 times does not result in measurable etching, suggesting that the etching is kinetically driven by the higher pressure doses at temperatures above 450 K or, possibly, that the etching is driven by impurities present in the HV setup. It does open up the possibility of controlling the etching rate by temperature and even of achieving ALE by thermal cycling.[52−55]

The key to designing an ALE process for complex materials is in the self-limiting nature of the half-cycles. At the same time, a full cycle has to result in complete removal of all of the components of complex (tertiary) materials. So far, surface chlorination and the formation of chemical bonds between the chromium and acac ligands are confirmed. However, how does the etching occur for the PS_4 fragments? A key comparison can

https://doi.org/10.1021/acs.chemmater.4c01606
Chem Mater XXXX XXX XXX−XXX

again be drawn between $CrPS_4$ and the previously studied CoFeB alloy ALE.[30] It was initially assumed that Co and Fe components would form acetylacetonates, and if chlorination is used, boron would be removed as BCl_3. However, it was discovered that the formation of true acetylacetonates of the transition metals occurred at temperatures much higher than the ALE processing conditions and that all of the elements, including boron, were removed as $M(acac)_x(Cl)_y$ compounds.[26,29−33] That was especially surprising for the light element boron. If PS_4 fragments are to be removed by interacting with chlorine or acac ligands, one must confirm that surface species containing P, S, and corresponding ligands can be formed on the surface of $CrPS_4$ flakes. The ToF-SIMS surface spectra presented in Figure 7 reveal signatures of

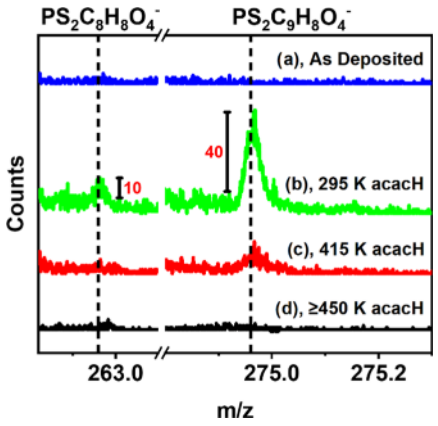

Figure 7 ToF-SIMS surface spectra of m/z ranges corresponding to $PS_2C_8H_8O_4^-$ and $PS_2C_9H_8O_4^-$. Spectra are provided for (a) the as-deposited $CrPS_4$ flakes, and (b) flakes after dosing acacH at room temperature, (c) 415 K, and (d) ≥ 450 K (controlling precise surface temperature above 450 K was challenging, and the actual surface temperature in this experiment is between 450 and 500 K). The black-dashed reference lines specify the exact m/z for each of the indicated species (262.960 and 274.960).

several species containing PS_2 and acac simultaneously. More interestingly, in this case, these complex species are formed immediately upon acacH adsorption at room temperature. In fact, the intensity of the corresponding features decreases dramatically even by the time the surface temperature reaches 415 K, and no intensity is recorded by 450 K. Thus, PS_2 fragments not only participate in the chemical modification of $CrPS_4$ with acacH but also appear to form surface fragments that are removed more easily than those containing chromium, offering the possibility of an efficient thermal ALE process based on self-limiting chromium removal.

Thus, the chemistry of the $CrPS_4$ surface with individual half-cycle reactants with the potential to be coreactants for thermal $CrPS_4$ ALE suggests that

(1) Both Cl_2 and acacH, when dosed individually, chemically modify the surface of $CrPS_4$;
(2) Cr-acac bonding is confirmed, but the formation of a stable $Cr(acac)_3$ compound is not recorded within the target temperature range (although the formation may be possible when the temperature is raised above 450 K), providing a self-saturation pathway with acacH and the possibility of mixed-ligand compound formation within a controlled temperature range;
(3) PS_2 fragment is also a clear part of surface modification with acacH, and it appears that the resulting fragments are thermally easier to remove than Cr-containing ones.

Overall, this summary suggests that it is possible to design thermal ALE for $CrPS_4$ and that the target of controlling the self-limiting process should be the removal of chromium.

Thermal Atomic Layer Etching. There are several targets of the thermal ALE of $CrPS_4$. The most obvious one is the control of the thickness of the flakes. However, the second objective is to reduce the size and quantity of defects on the exfoliated flakes. Thermal ALE is well-known to result in smoother surfaces compared to the starting ones.[21,27,28] So, in addition to the main goal, we aim at examining the effect of ALE on the surface defects created by the exfoliation.

Figure 8 summarizes the AFM results after a representative ALE experiment was performed on $CrPS_4$ flakes exfoliated on an Au support surface. The as-deposited structure in this image has three representative regions: a relatively thick flake with clear terraces; the defects created on top of these terraces during exfoliation (islands of approximately 5 nm in height); and very thin layers of approximately 4 nm with holes tens of nanometers in width created during mechanical exfoliation. One would aim to eliminate the defects and also to control the thickness of the flakes using ALE, so the relatively thick areas and defective features should be examined individually.

Thirty ALE cycles were completed at 450 K in UHV and resulted in 0.10 ± 0.07 nm/cycle based on 75 AFM line scans from multiple flakes of each type across the sample. Figure 8 shows a representative image with the main types of surface structures investigated and subjected to ALE. The terraces of the relatively thick (tens of nanometers) flakes are etched the slowest at 0.07 ± 0.04 nm/cycle. This is illustrated in part A of Figure 8. The island defects (also shown in part A of Figure 8) and the relatively thin few-nanometer-thick flakes with a high density of hole defects shown for part B in Figure 8 are etched at a rate of 0.15 ± 0.02 nm/cycle. In these images, the highly defective areas are almost completely removed by 30 ALE cycles. The etching rate was also confirmed by varying the number of cycles up to 45.

Part C of Figure 8 zooms into the defect-free area of the flake, where the terrace features are clearly observed. It is interesting to note that even though the defect islands are removed by the ALE treatment, the terraces at different steps are etched at the same rate as all of the step features appear to be fully maintained. Of course, the resolution of AFM does not allow for a reliable comparison of the etching rates of the step edges and terraces; however, it is clear that the step structure is maintained.

Thus, following ALE in UHV, the flakes become smoother because the defective areas are etched faster than the main terraces, and, at the same time, the step structure of the crystalline flakes is maintained.

In the work described in this article, the flakes were exfoliated on either Au-coated silica or uncoated silicon wafers, and the thickness of the flakes investigated was assumed to be sufficiently high to consider any possible substrate-dependent ALE effects are negligible. The effects of the substrates on the etching rate of the thin (few-nanometer thick) flakes are a subject of ongoing work; however, exfoliating the flakes on the Au surface allows for a preliminary assessment of the produced interfaces. The Au surface appears to become slightly rougher following the ALE treatment (RMS roughness 0.33 nm before

https://doi.org/10.1021/acs.chemmater.4c01606
Chem Mater XXXX XXX XXX−XXX

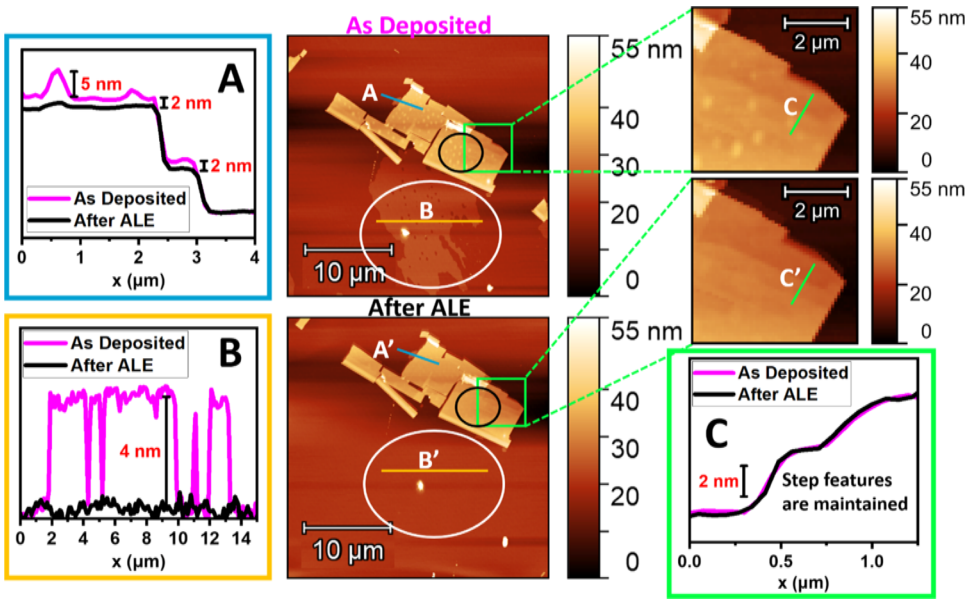

Figure 8 AFM images for $CrPS_4$ flakes before and after 30 ALE cycles at 450 K. Each plot gives the line profile before (pink) and after (black) ALE in UHV. (A) Island defects atop the terrace of the thicker flake were 2−5 nm after deposition and were almost completely removed after ALE. The terrace of the thicker flake was etched 2 nm after 30 cycles, suggesting that it is etched at a slower rate compared to the defects. (B) Few-layer thick flake area, which was 4 nm thick after deposition, is almost completely removed after ALE. (C) Structure of the steps on the surface of the thick flake is preserved. The black circles in the central images highlight the island defects that are removed after ALE. The white circles highlight the few-layer thick flake that is almost completely removed after ALE.

30 cycles of ALE vs 0.39 nm after ALE); however, the gold surface protected by the $CrPS_4$ flakes may be unaffected by the conditions of the experiment.

To further investigate this effect, a different ALE experiment, which used much higher dosing pressures, was performed on a $CrPS_4$ sample. After the ALE experiment, 2 μm of Cu was deposited over the sample as a protective layer. Then, a cross-sectional TEM sample of a $CrPS_4$ flake was prepared by using FIB-SEM. The resulting image is shown in Figure 9. This experiment indeed confirms that the interface between the $CrPS_4$ flake and the gold-covered substrate does not exhibit any noticeable changes and is protected by the flake.

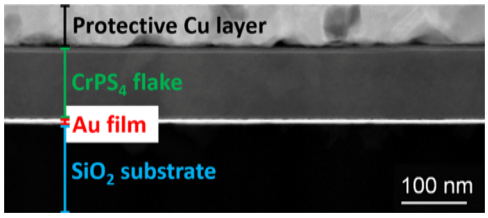

Figure 9 Cross-sectional TEM images of a $CrPS_4$ flake after ALE, along with the underlying Au film and SiO_2 wafer. The Au protected by $CrPS_4$ remained flat, continuous, and intact. The 2 μm layer of copper was deposited after ALE experiments to protect the flake from damage by the FIB-SEM.

Overall, it is not expected that the etching of the underlying substrate plays any substantial role in our experiments. Although gold ALE with chlorination and subsequent dose of triethylphosphine (PEt_3) has been reported at elevated temperatures and mTorr pressure range, a very specific Au^+ etching product, $AuClPEt_3$, was recorded.[56] The formation of this type of product is not expected in our case, but we confirmed the absence of appreciable gold removal in our ALE process by comparing the survey XPS spectra before and after ALE and analyzing the ratios of Au signal to those of underlying substrates. Oxidized silicon used in selected experiments as a substrate has also been shown not to be etched by the process.[30]

The ALE regime was demonstrated for $CrPS_4$ at 450 K, and it was also shown that at higher temperatures and higher reagent exposures, the etching could occur at a substantially higher rate without self-limited half-cycle reactions. However, ToF-SIMS tests also suggested that surface species that are key to the material removal are formed on its surface at temperatures as low as 415 K. To test the temperature window of ALE processing, 30 ALE cycles were performed on a $CrPS_4$ flake sample on Au at 420 K. However, the experiment summarized in Figure 10 did not result in any significant etching. Even the defect islands on top of the $CrPS_4$ flakes were not removed, showing that the $CrPS_4$ ALE is highly temperature-dependent.

SUMMARY AND CONCLUSIONS

We have shown that, based on ToF-SIMS, the surface of $CrPS_4$ flakes can be chlorinated. Additionally, acacH interacts with the $CrPS_4$ surface at 295 and 415 K but does not result in measurable etching. The etching is indeed achieved at temperatures above 450 K in high vacuum at high exposures of acacH, but this regime is not self-limiting. A similar experiment in UHV using an acacH partial pressure of 5×10^{-6} Torr at 450 K does not result in measurable etching. Using Cl_2 in combination with acacH results in a controllable self-limiting process. This process is highly temperature-dependent, with no discernible etching occurring at 420 K. Not even defect island areas are observed to be changed at this temperature.

When ALE cycles are completed at 450 K in UHV with Cl_2 dosed for the first half-cycle, the $CrPS_4$ flake etching rate is

https://doi.org/10.1021/acs.chemmater.4c01606
Chem Mater XXXX XXX XXX−XXX

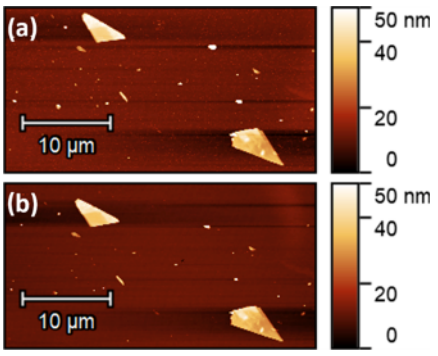

Figure 10 AFM images of $CrPS_4$ flakes before (a) and after (b) 30 ALE cycles at 420 K. None of the features, not even the defect ad-islands on the flake surface, are removed, suggesting that ALE cycles at this temperature will not result in any etching.

0.10 ± 0.07 nm/cycle. Thinner flakes and defects are etched fastest (over 4 nm after 30 ALE cycles, 0.15 ± 0.02 nm/cycle), and terraces are etched slower (~2 nm after 30 ALE cycles, 0.7 ± 0.4 nm/cycle). Because of the faster etching rate for defects, the ALE regime presented here can be used to achieve an atomically flat $CrPS_4$ surface. The proposed ALE process does not substantially affect the step structure of the surface.

Thus, we have shown that thermal ALE can be used to control the thickness of 2D TTMC $CrPS_4$ with atomic-level precision. This approach is amenable to creating structures of controlled numbers of layers of $CrPS_4$, which will allow its unique physical properties to be studied. Further work is required to investigate the ALE control for few-layer thick 2D materials and to investigate the effect of the substrate on both the material properties and the interface between the substrate and TTMC.

■ ASSOCIATED CONTENT

Supporting Information

The Supporting Information is available free of charge at https://pubs.acs.org/doi/10.1021/acs.chemmater.4c01606.

Additional ToF-SIMS experiments (PDF)

■ AUTHOR INFORMATION

Corresponding Author

Andrew V Teplyakov − *Department of Chemistry and Biochemistry University of Delaware Newark Delaware 19716 United States;* orcid.org/0000-0002-6646-3310; Email: andrewt@udel.edu

Authors

Marissa D Pina − *Department of Chemistry and Biochemistry University of Delaware Newark Delaware 19716 United States*

Matthew P Whalen − *Quantum Science and Engineering Program University of Delaware Newark Delaware 19716 United States*

John Q Xiao − *Department of Physics and Astronomy University of Delaware Newark Delaware 19716 United States;* orcid.org/0000-0001-7805-8155

Complete contact information is available at: https://pubs.acs.org/10.1021/acs.chemmater.4c01606

Author Contributions

The manuscript was written through contributions of all authors. All authors have given approval to the final version of the manuscript.

Notes

The authors declare no competing financial interest.

■ ACKNOWLEDGMENTS

This work was supported by the National Science Foundation (CMMI-2035154, CMMI-2225900). TOF-SIMS is sponsored by the National Science Foundation, Major Research Instrumentation, Award Number: DMR-2116754.

■ REFERENCES

(1) Zou, X.; Xu, Y.; Duan, W. 2D Materials: Rising Star for Future Applications. *Innovation* **2021**, *2* (2), No. 100115.

(2) Schulz, S.; Nechaev, I. A.; Guttler, M.; Poelchen, G.; Generalov, A.; Danzenbächer, S.; Chikina, A.; Seiro, S.; Kliemt, K.; Vyazovskaya, A. Y.; Kim, T. K.; Dudin, P.; Chulkov, E. V.; Laubschat, C.; Krasovskii, E. E.; Geibel, C.; Krellner, C.; Kummer, K.; Vyalikh, D. V. Emerging 2D-Ferromagnetism and Strong Spin-Orbit Coupling at the Surface of Valence-Fluctuating $EuIr_2Si_2$. *npj Quantum Mater.* **2019**, *4*, 26.

(3) Deng, J.; Guo, J.; Hosono, H.; Ying, T.; Chen, X. Two-Dimensional Bipolar Ferromagnetic Semiconductors from Layered Antiferromagnets. *Phys. Rev. Mater.* **2021**, *5* (3), No. 034005.

(4) Fan, F. R.; Wang, R.; Zhang, H.; Wu, W. Emerging Beyond-Graphene Elemental 2D Materials for Energy and Catalysis Applications. *Chem. Soc. Rev.* **2021**, *50* (19), 10983−11031.

(5) Son, J.; Son, S.; Park, P.; Kim, M.; Tao, Z.; Oh, J.; Lee, T.; Lee, S.; Kim, J.; Zhang, K.; Cho, K.; Kamiyama, T.; Lee, J. H.; Mak, K. F.; Shan, J.; Kim, M.; Park, J. G.; Lee, J. Air-Stable and Layer-Dependent Ferromagnetism in Atomically Thin van Der Waals $CrPS_4$. *ACS Nano* **2021**, *15* (10), 16904−16912.

(6) Lee, J.; Ko, T. Y.; Kim, J. H.; Bark, H.; Kang, B.; Jung, S. G.; Park, T.; Lee, Z.; Ryu, S.; Lee, C. Structural and Optical Properties of Single- and Few-Layer Magnetic Semiconductor $CrPS_4$. *ACS Nano* **2017**, *11* (11), 10935−10944.

(7) Bo, X.; Li, F.; Yin, X.; Chen, Y.; Wan, X.; Pu, Y. Magnetic Structure and Exchange Interactions of the van Der Waals $CrPS_4$ Monolayer under Strain: A First-Principles Study. *Phys. Rev. B* **2023**, *108* (2), No. 024405.

(8) Peng, Y.; Ding, S.; Cheng, M.; Hu, Q.; Yang, J.; Wang, F.; Xue, M.; Liu, Z.; Lin, Z.; Avdeev, M.; Hou, Y.; Yang, W.; Zheng, Y.; Yang, J. Magnetic Structure and Metamagnetic Transitions in the van Der Waals Antiferromagnet $CrPS_4$. *Adv. Mater.* **2020**, *32* (28), No. 2001200.

(9) Yin, L.; Cheng, R.; Ding, J.; Jiang, J.; Hou, Y.; Feng, X.; Wen, Y.; He, J. Two-Dimensional Semiconductors and Transistors for Future Integrated Circuits. *ACS Nano* **2024**, *18* (11), 7739−7768.

(10) Velicky, M.; Donnelly, G. E.; Hendren, W. R.; McFarland, S.; Scullion, D.; DeBenedetti, W. J. I.; Correa, G. C.; Han, Y.; Wain, A. J.; Hines, M. A.; Muller, D. A.; Novoselov, K. S.; Abruna, H. D.; Bowman, R. M.; Santos, E. J. G.; Huang, F. Mechanism of Gold-Assisted Exfoliation of Centimeter-Sized Transition-Metal Dichalcogenide Monolayers. *ACS Nano* **2018**, *12* (10), 10463−10472.

(11) Budniak, A. K.; Killilea, N. A.; Zelewski, S. J.; Sytnyk, M.; Kauffmann, Y.; Amouyal, Y.; Kudrawiec, R.; Heiss, W.; Lifshitz, E. Exfoliated $CrPS_4$ with Promising Photoconductivity. *Small* **2020**, *16* (1), No. 1905924.

(12) Li, Z.; Ren, L.; Wang, S.; Huang, X.; Li, Q.; Lu, Z.; Ding, S.; Deng, H.; Chen, P.; Lin, J.; Hu, Y.; Liao, L.; Liu, Y. Dry Exfoliation of Large-Area 2D Monolayer and Heterostructure Arrays. *ACS Nano* **2021**, *15* (8), 13839−13846.

(13) Desai, S. B.; Madhvapathy, S. R.; Amani, M.; Kiriya, D.; Hettick, M.; Tosun, M.; Zhou, Y.; Dubey, M.; Ager, J. W.; Chrzan, D.;

Javey, A. Gold-Mediated Exfoliation of Ultralarge Optoelectronically-Perfect Monolayers. *Adv. Mater.* **2016**, *28* (21), 4053−4058.
(14) Heyl, M.; List-Kratochvil, E. J. W. Only Gold Can Pull This off: Mechanical Exfoliations of Transition Metal Dichalcogenides beyond Scotch Tape. *Appl. Phys. A: Mater. Sci. Process.* **2023**, *129*, 16.
(15) Heyl, M.; Burmeister, D.; Schultz, T.; Pallasch, S.; Ligorio, G.; Koch, N.; List-Kratochvil, E. J. W. Thermally Activated Gold-Mediated Transition Metal Dichalcogenide Exfoliation and a Unique Gold-Mediated Transfer. *Phys. Status Solidi RRL* **2020**, *14* (11), No. 2000408.
(16) Magda, G. Z.; Pető, J.; Dobrik, G.; Hwang, C.; Biró, L. P.; Tapasztó, L. Exfoliation of Large-Area Transition Metal Chalcogenide Single Layers. *Sci. Rep.* **2015**, *5*, No. 14714.
(17) Liu, F.; Wu, W.; Bai, Y.; Chae, S. H.; Li, Q.; Wang, J.; Hone, J.; Zhu, X.-Y. Disassembling 2D van Der Waals Crystals into Macroscopic Monolayers and Reassembling into Artificial Lattices. *Science* **2020**, *367* (6480), 903−906.
(18) Huang, Y.; Pan, Y.-H.; Yang, R.; Bao, L.-H.; Meng, L.; Luo, H.-L.; Cai, Y.-Q.; Liu, G.-D.; Zhao, W.-J.; Zhou, Z.; Wu, L.-M.; Zhu, Z.-L.; Huang, M.; Liu, L.-W.; Liu, L.; Cheng, P.; Wu, K.-H.; Tian, S.-B.; Gu, C.-Z.; Shi, Y.-G.; Guo, Y.-F.; Cheng, Z. G.; Hu, J.-P.; Zhao, L.; Yang, G.-H.; Sutter, E.; Sutter, P.; Wang, Y.-L.; Ji, W.; Zhou, X.-J.; Gao, H.-J. Universal Mechanical Exfoliation of Large-Area 2D Crystals. *Nat. Commun.* **2020**, *11*, No. 2453.
(19) Wang, X.; Gong, Y.; Shi, G.; Chow, W. L.; Keyshar, K.; Ye, G.; Vajtai, R.; Lou, J.; Liu, Z.; Ringe, E.; Tay, B. K.; Ajayan, P. M. Chemical Vapor Deposition Growth of Crystalline Monolayer $MoSe_2$. *ACS Nano* **2014**, *8* (5), 5125−5131.
(20) Lee, M. J.; Lee, S.; Lee, S.; Balamurugan, K.; Yoon, C.; Jang, J. T.; Kim, S.-H.; Kwon, D.-H.; Kim, M.; Ahn, J.-P.; Kim, D. H.; Park, J.-G.; Park, B. H. Synaptic Devices Based on Two-Dimensional Layered Single-Crystal Chromium Thiophosphate ($CrPS_4$). *NPG Asia Mater.* **2018**, *10* (4), 23−30.
(21) Kanarik, K. J.; Tan, S.; Gottscho, R. A. Atomic Layer Etching: Rethinking the Art of Etch. *J. Phys. Chem. Lett.* **2018**, *9* (16), 4814−4821.
(22) Pham, P. V.; Mai, T.-H.; Do, H.-B.; Vasundhara, M.; Nguyen, V.-H.; Nguyen, T.; Bui, H.; Van; Dao, V.-D.; Gupta, R. K.; Ponnusamy, V. K.; Park, J.-H. Layer-by-Layer Thinning of Two-Dimensional Materials. *Chem. Soc. Rev.* **2024**, *53* (10), 5190−5226.
(23) Hoffman, A. N.; Gu, Y.; Tokash, J.; Woodward, J.; Xiao, K.; Rack, P. D. Layer-by-Layer Thinning of $PdSe_2$ Flakes via Plasma Induced Oxidation and Sublimation. *ACS Appl. Mater. Interfaces* **2020**, *12* (6), 7345−7350.
(24) Soares, J.; Mane, A. U.; Choudhury, D.; Letourneau, S.; Hues, S. M.; Elam, J. W.; Graugnard, E. Thermal Atomic Layer Etching of MoS_2 Using MoF_6 and H_2O. *Chem. Mater.* **2023**, *35* (3), 927−936.
(25) Wang, Z.; Li, Q.; Xu, H.; Dahl-Petersen, C.; Yang, Q.; Cheng, D.; Cao, D.; Besenbacher, F.; Lauritsen, J. V.; Helveg, S.; Dong, M. Controllable Etching of MoS_2 Basal Planes for Enhanced Hydrogen Evolution through the Formation of Active Edge Sites. *Nano Energy* **2018**, *49*, 634−643.
(26) Konh, M.; Wang, Y.; Pina, M.; Teplyakov, A. V.; Xiao, J. Q. Effects of Atomic Layer Etching on Magnetic Properties of CoFeB Films: Reduction of Gilbert Damping. *J. Magn. Magn. Mater.* **2022**, *564* (2), No. 170052.
(27) Kanarik, K. J.; Lill, T.; Hudson, E. A.; Sriraman, S.; Tan, S.; Marks, J.; Vahedi, V.; Gottscho, R. A. Overview of Atomic Layer Etching in the Semiconductor Industry. *J. Vac. Sci. Technol. A* **2015**, *33* (2), No. 020802.
(28) Fischer, A.; Routzahn, A.; George, S. M.; Lill, T. Thermal Atomic Layer Etching: A Review. *J. Vac. Sci. Technol. A* **2021**, *39* (3), No. 030801.
(29) Konh, M.; Janotti, A.; Teplyakov, A. Molecular Mechanism of Thermal Dry Etching of Iron in a Two-Step Atomic Layer Etching Process: Chlorination Followed by Exposure to Acetylacetone. *J. Phys. Chem. C* **2021**, *125* (13), 7142−7154.
(30) Konh, M.; Wang, Y.; Chen, H.; Bhatt, S.; Xiao, J. Q.; Teplyakov, A. V. Selectivity in Atomically Precise Etching: Thermal Atomic Layer Etching of a CoFeB Alloy and Its Protection by MgO. *Appl. Surf. Sci.* **2022**, *575*, No. 151751.
(31) Zhao, J.; Konh, M.; Teplyakov, A. Surface Chemistry of Thermal Dry Etching of Cobalt Thin Films Using Hexafluoroacetylacetone (HfacH). *Appl. Surf. Sci.* **2018**, *455*, 438−445.
(32) Konh, M.; He, C.; Lin, X.; Guo, X.; Pallem, V.; Opila, R. L.; Teplyakov, A. V.; Wang, Z.; Yuan, B. Molecular Mechanisms of Atomic Layer Etching of Cobalt with Sequential Exposure to Molecular Chlorine and Diketones. *J. Vac. Sci. Technol. A* **2019**, *37* (2), No. 021004.
(33) Wang, Z.; Opila, R. L. *In Operando* X-ray Photoelectron Spectroscopy Study of Mechanism of Atomic Layer Etching of Cobalt. *J. Vac. Sci. Technol. A* **2020**, *38* (2), No. 022611.
(34) Pankajavalli, R.; Mallika, C.; Sreedharan, O. M.; Raghunathan, V. S.; Antony Premkumar, P.; Nagaraja, K. S. Thermal Stability of Organo-Chromium or Chromium Organic Complexes and Vapor Pressure Measurements on Tris(2,4-Pentanedionato)Chromium(III) and Hexacarbonyl Chromium(0) by TG-Based Transpiration Method. *Chem. Eng. Sci.* **2002**, *57* (17), 3603−3610.
(35) Rippy, K.; Witteman, L.; Taylor, P. R.; Vidal, J. C. Predicting and Understanding Corrosion in Molten Chloride Salts. *MRS Adv.* **2023**, *8*, 855−859.
(36) Spencer, N. D.; Goddard, P. J.; Davies, P. W.; Kitson, M.; Lambert, R. M. A Simple, Controllable Source for Dosing Molecular Halogens in UHV. *J. Vac. Sci. Technol. A* **1983**, *1* (3), 1554−1555.
(37) Farzaneh, A.; Butera, R. E. Si Epitaxy on Cl-Si(100). *Appl. Surf. Sci.* **2022**, *589*, No. 152877.
(38) Stein, S. E. IR and Mass Spectra. In *NIST Chemistry WebBook*; NIST Standard Reference Database Number 69; National Institute of Standards and Technology: Gaithersburg, MD, 2000.
(39) Fairley, N.; Fernandez, V.; Richard-Plouet, M.; Guillot-Deudon, C.; Walton, J.; Smith, E.; Flahaut, D.; Greiner, M.; Biesinger, M.; Tougaard, S.; Morgan, D.; Baltrusaitis, J. Systematic and Collaborative Approach to Problem Solving Using X-Ray Photoelectron Spectroscopy. *Appl. Surf. Sci. Adv.* **2021**, *5*, No. 100112.
(40) Ohno, Y.; Mineo, A.; Matsubara, I. Reflection Electron-Energy-Loss Spectroscopy, X-ray-Absorption Spectroscopy, and x-Ray Photoelectron Spectroscopy Studies of a New Type of Layer Compound $CrPS_4$. *Phys. Rev. B* **1989**, *40* (15), 10262−10272.
(41) Edmonds, M. T.; Tadich, A.; Carvalho, A.; Ziletti, A.; O'Donnell, K. M.; Koenig, S. P.; Coker, D. F.; Ozyilmaz, B.; Neto, A. H. C.; Fuhrer, M. S. Creating a Stable Oxide at the Surface of Black Phosphorus. *ACS Appl. Mater. Interfaces* **2015**, *7* (27), 14557−14562.
(42) Glorieux, B.; Berjoan, R.; Matecki, M.; Kammouni, A.; Perarnau, D. XPS Analyses of Lanthanides Phosphates. *Appl. Surf. Sci.* **2007**, *253* (6), 3349−3359.
(43) Wang, Y.; Asunskis, D. J.; Sherwood, P. M. A. Iron (II) Phosphate ($Fe_3(PO_4)_2$ by XPS. *Surf. Sci. Spectra* **2002**, *9* (1), 91−98.
(44) Felker, D. L.; Sherwood, P. M. A. Zinc Phosphate ($Zn_3(PO_4)_2$) by XPS. *Surf. Sci. Spectra* **2002**, *9* (1), 106−113.
(45) Rotole, J. A.; Sherwood, P. M. A. Aluminum Metaphosphate ($Al(PO_3)_3$) by XPS. *Surf. Sci. Spectra* **1998**, *5* (1), 67−74.
(46) Brow, R. K. An XPS Study of Oxygen Bonding in Zinc Phosphate and Zinc Borophosphate Glasses. *J. Non-Cryst. Solids* **1996**, *194* (3), 267−273.
(47) Wu, Z.; Huang, L.; Liu, H.; Li, M.; Wang, H. Surface Oxidation of Transition Metal Sulfide and Phosphide Nanomaterials. *Nano Res.* **2021**, *14* (7), 2264−2267.
(48) Hampton, M. A.; Plackowski, C.; Nguyen, A. V. Physical and Chemical Analysis of Elemental Sulfur Formation during Galena Surface Oxidation. *Langmuir* **2011**, *27* (7), 4190−4201.
(49) Xie, L.; Wang, J.; Li, J.; Li, C.; Zhang, Y.; Zhu, B.; Guo, Y.; Wang, Z.; Zhang, K. An Atomically Thin Air-Stable Narrow-Gap Semiconductor Cr_2S_3 for Broadband Photodetection with High Responsivity. *Adv. Electron. Mater.* **2021**, *7* (7), No. 2000962.
(50) Laajalehto, K.; Kartio, I.; Nowak, P. XPS Study of Clean Metal Sulfide Surfaces. *Appl. Surf. Sci.* **1994**, *81* (1), 11−15.
(51) Larrabure, G.; Chero-Osorio, S.; Silva-Quinones, D.; Benndorf, C.; Williams, M.; Gao, F.; Gamarra, C.; Alarcón, A.; Segura, C.;

https://doi.org/10.1021/acs.chemmater.4c01606
Chem Mater XXXX XXX XXX−XXX

Teplyakov, A.; Rodriguez-Reyes, J. C. F. Surface Processes at a Polymetallic (Mn-Fe-Pb) Sulfide Subject to Cyanide Leaching under Sonication Conditions and with an Alkaline Pretreatment: Understanding Differences in Silver Extraction with X-Ray Photoelectron Spectroscopy (XPS). *Hydrometallurgy* **2021**, *200*, No. 105544.
(52) Shinoda, K.; Miyoshi, N.; Kobayashi, H.; Izawa, M.; Ishikawa, K.; Hori, M. Rapid Thermal-Cyclic Atomic-Layer Etching of Titanium Nitride in CHF_3O_2 Downstream Plasma. *J. Phys. D: Appl. Phys.* **2019**, *52*, No. 475106.
(53) Ikeda, K.; Imai, S.; Matsumura, M. Atomic Layer Etching of Germanium. *Appl. Surf. Sci.* **1997**, *112*, 87−91.
(54) Miyoshi, N.; Kobayashi, H.; Shinoda, K.; Kurihara, M.; Watanabe, T.; Kouzuma, Y.; Yokogawa, K.; Sakai, S.; Izawa, M. Atomic Layer Etching of Silicon Nitride Using Infrared Annealing for Short Desorption Time of Ammonium Fluorosilicate. *Jpn. J. Appl. Phys.* **2017**, *56* (6), No. 06HB01.
(55) Fujisaki, S.; Yamaguchi, Y.; Kobayashi, H.; Shinoda, K.; Yamada, M.; Kawamura, K.; Izawa, M. Oxidation State of Cobalt Oxide in Thermal-Cyclic Atomic Layer Etching of Cobalt by Plasma Oxidation and Organometallization. *AIP Adv.* **2024**, *14* (4), No. 045321.
(56) Partridge, J. L.; Murdzek, J. A.; Johnson, V. L.; Cavanagh, A. S.; Sharma, S.; George, S. M. Thermal Atomic Layer Etching of Gold Using Sulfuryl Chloride for Chlorination and Triethylphosphine for Ligand Addition. *Chem. Mater.* **2024**, *36* (10), 5149−5159.

https://doi.org/10.1021/acs.chemmater.4c01606
Chem Mater XXXX XXX XXX−XXX